Supplement of Ocean Sci., 21, 989–1002, 2025
https://doi.org/10.5194/os-21-989-2025-supplement

Ocean Science
Open Access

Supplement of

Turbulent erosion of a subducting intrusion in the Western Mediterranean Sea

Giovanni Testa et al.

Correspondence to: Giovanni Testa (giovanni.testa@ve.ismar.cnr.it)

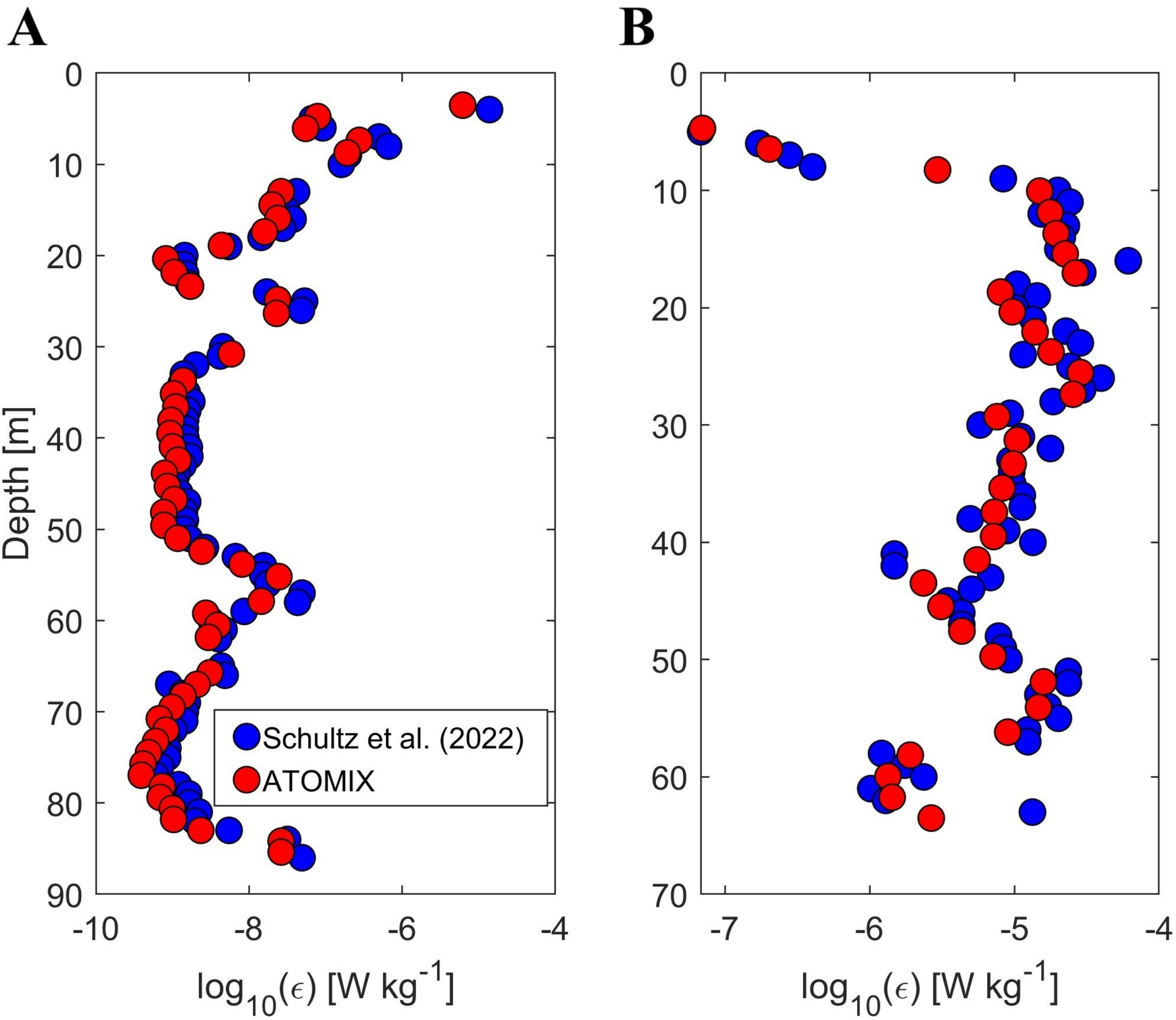

Figure S1. Profiles of turbulent kinetic energy dissipation rates from the ATOMIX dataset, collected in the Baltic Sea with an MSS90L profiler **(A)** and in the Haro Strait with a VMP250 instrument **(B)**. Level 2 ATOMIX data were processed using the Schulz et al. (2022) routines (blue points) and in accordance with ATOMIX best practices (red points).

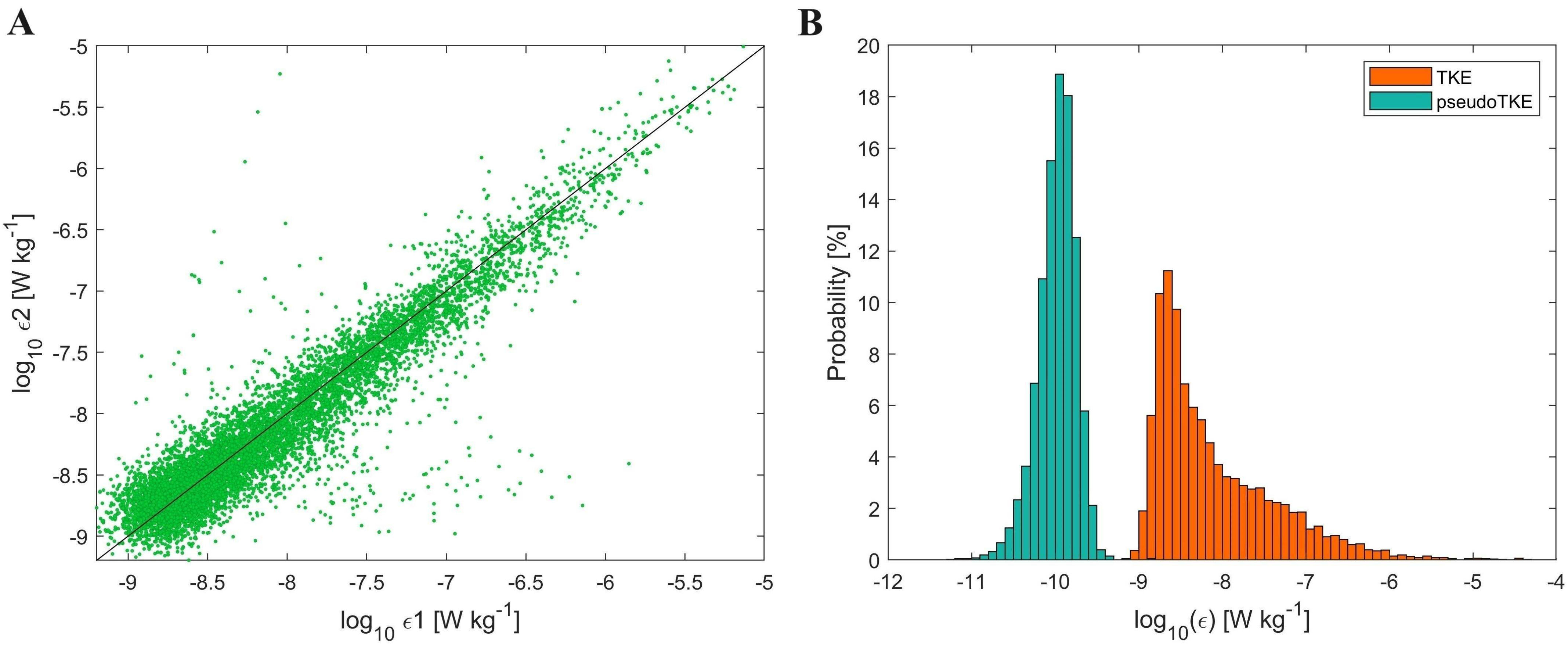

Figure S2. Turbulent dissipation rates (ε1 and ε2) recorded from both shear sensors (**A**) and probability distribution frequency for turbulent kinetic energy dissipation rates and pseudo dissipation rates **(B)**. The black solid line in panel (**A**) represents the 1:1 proportion between ε1 and ε2.

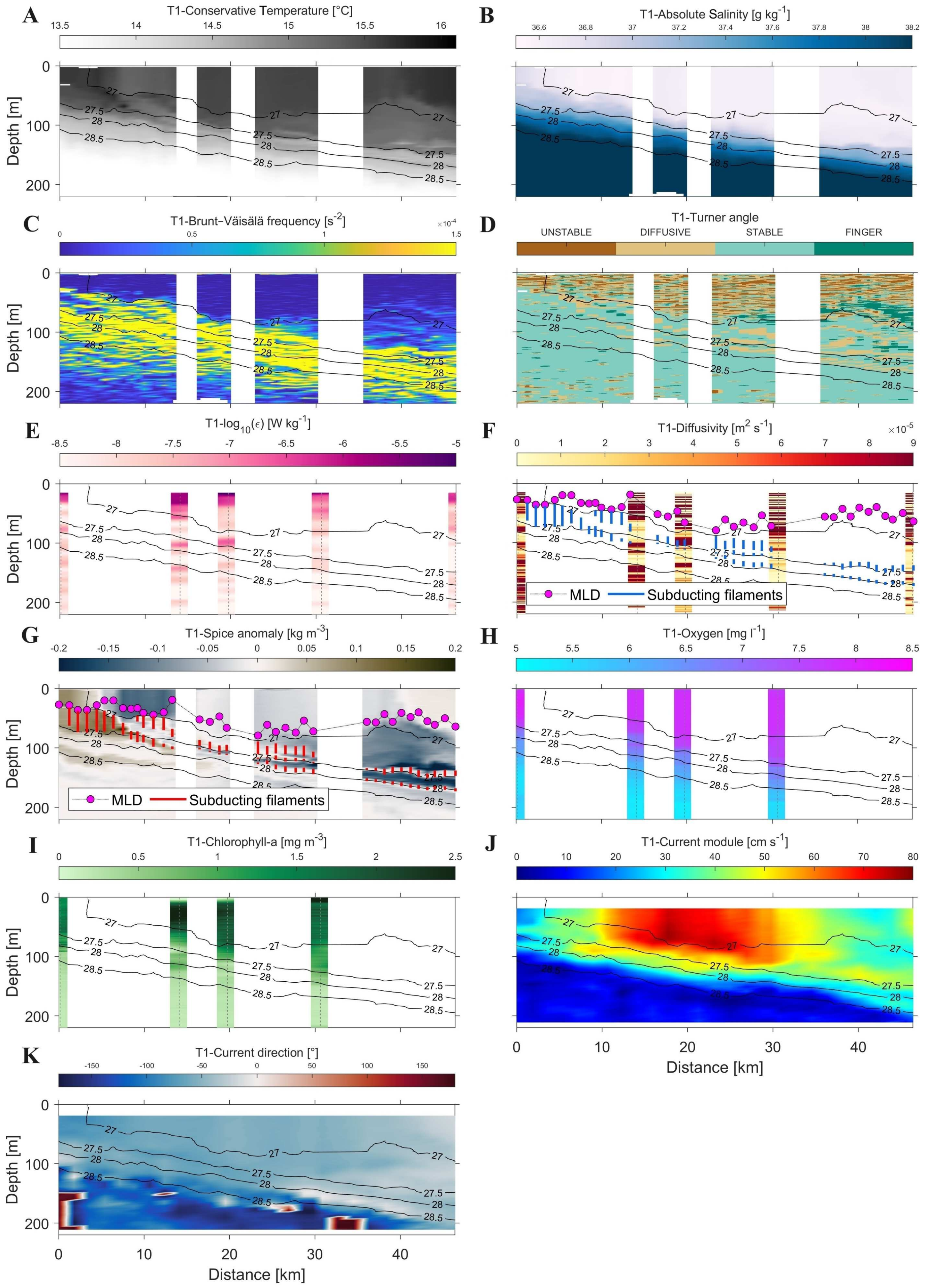

Figure S3. Conservative Temperature **(A)**, Absolute Salinity **(B)**, Brunt–Väisälä frequency **(C)**, Turner angle **(D)**, turbulent kinetic energy dissipation rates **(E)**, diffusivity **(F)**, spice anomaly **(G)**, dissolved oxygen **(H)**, chlorophyll-a **(I)**, current module **(J)** and direction **(K)** estimations along the transect 1 of the 2019 CALYSPSO campaign. Black lines represent the density anomaly isopycnals, whereas the grey dashed lines indicate the microstructure sampling stations location. The distance between stations was calculated starting from the sampling point located to the east.

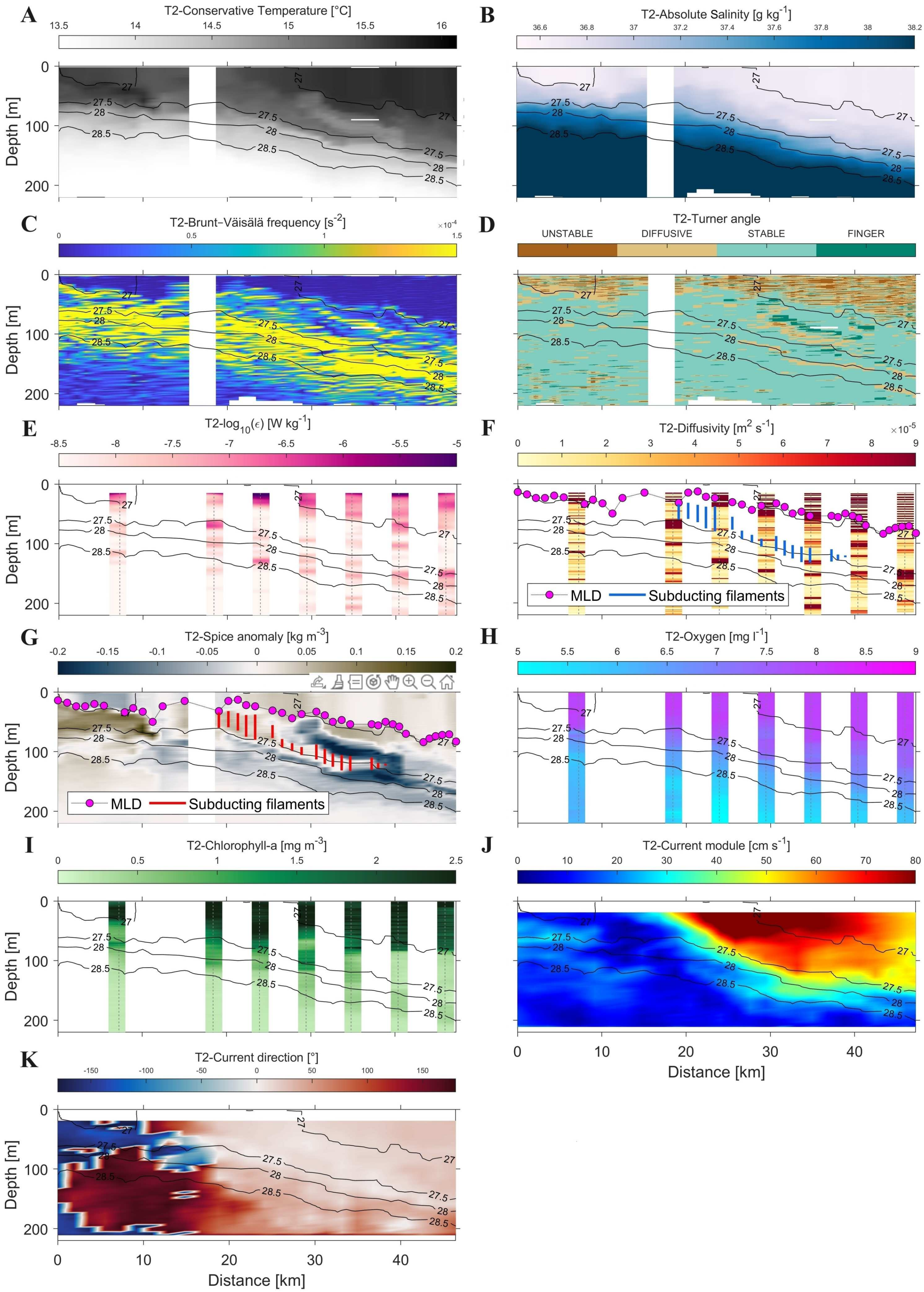

Figure S4. Same as Figure S3 but for transect 2 of the 2019 CALYPSO campaign. The distance between stations was calculated starting from the sampling point located to the north.

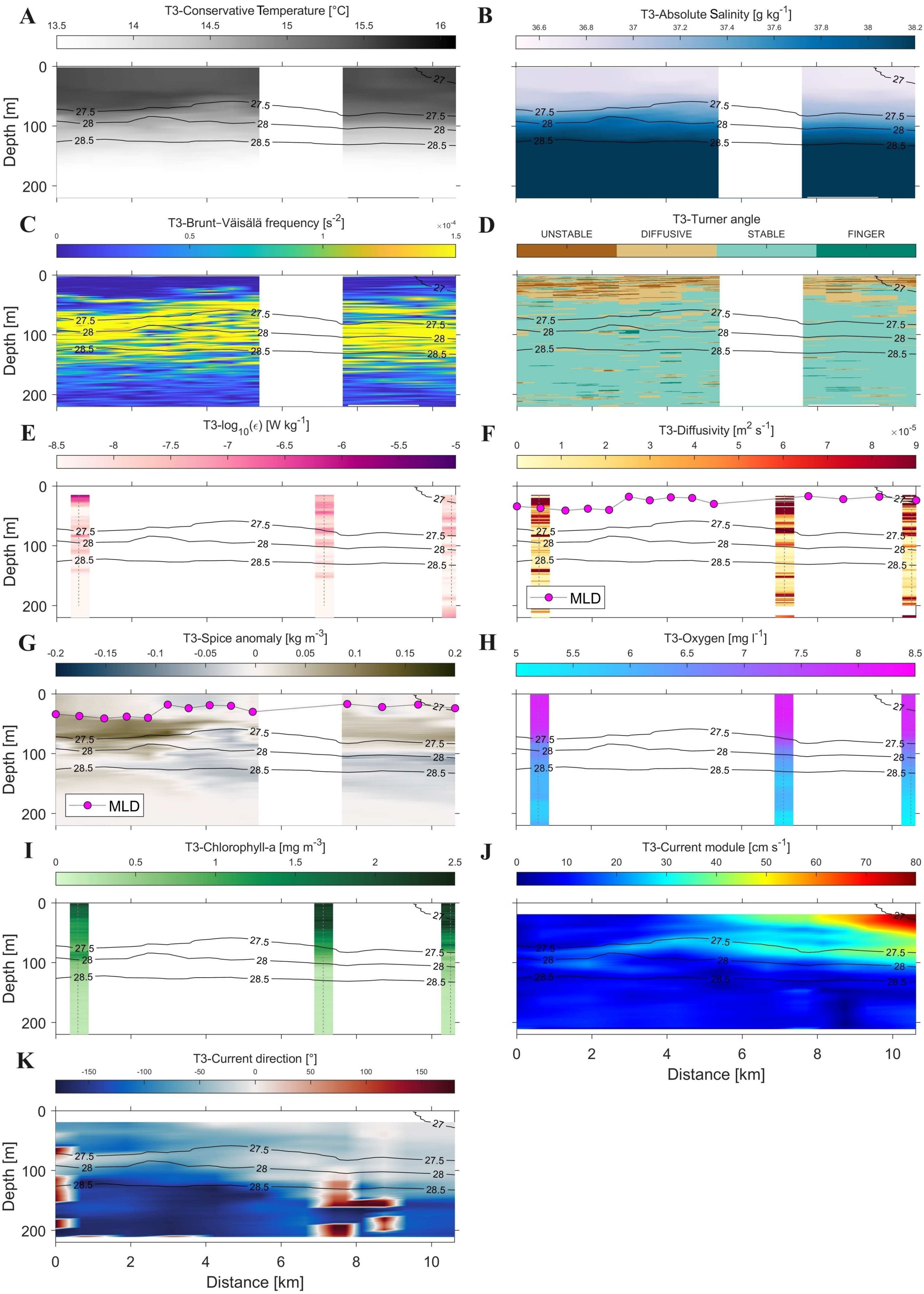

Figure S5. Same as Figure S4 but for transect 3 of the 2019 CALYPSO campaign.

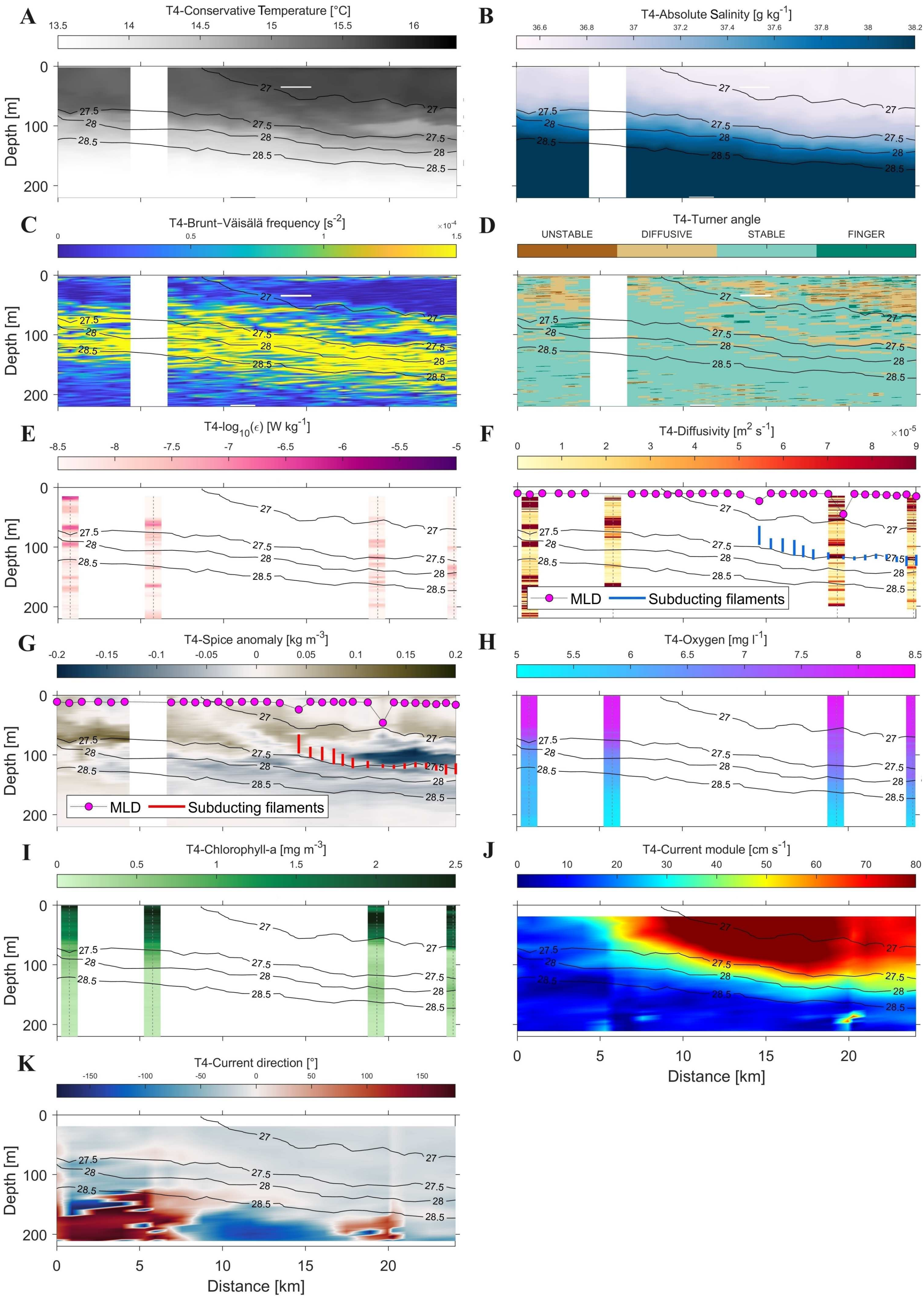

Figure S6. Same as Figure S4 but for transect 4 of the 2019 CALYPSO campaign.

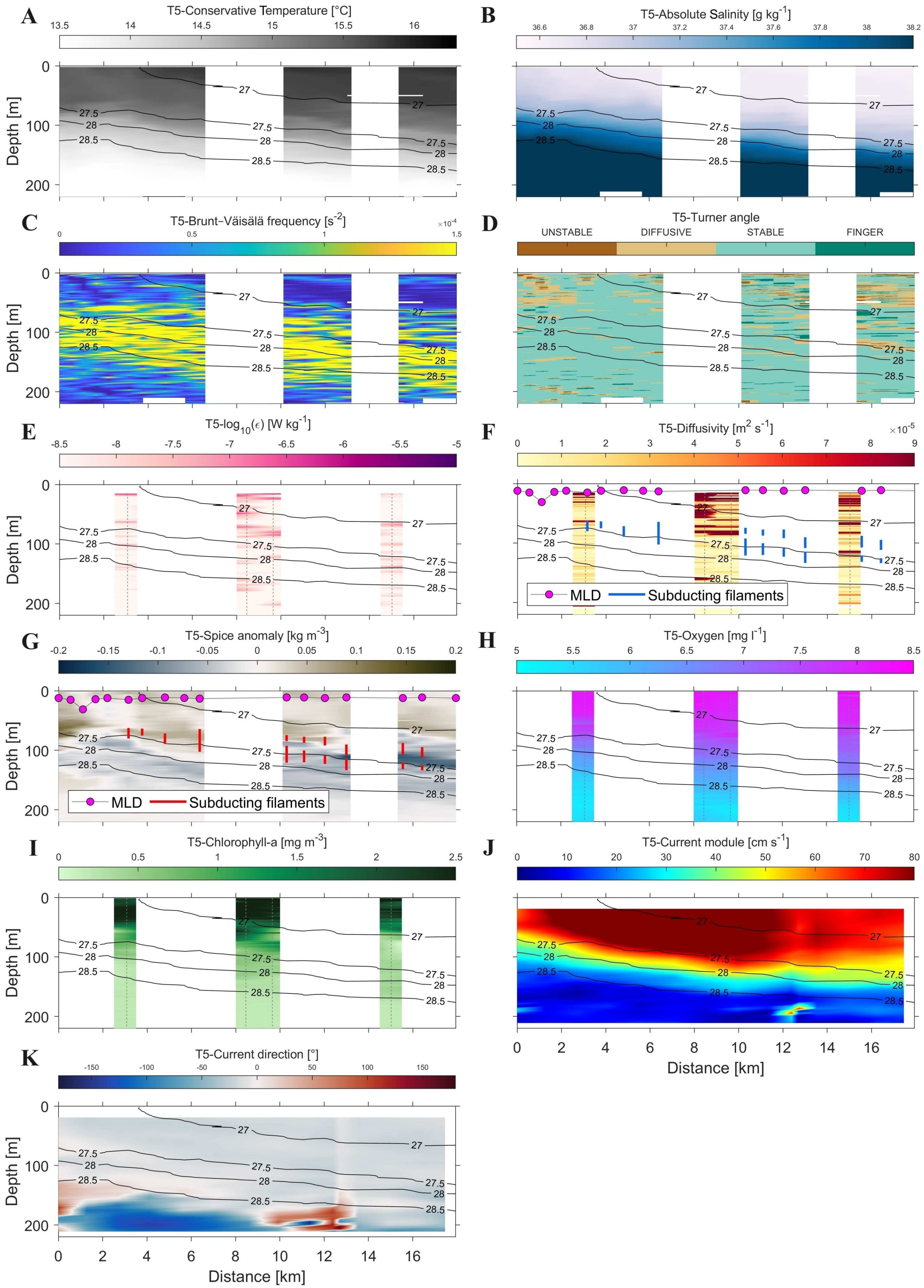

Figure S7. Same as Figure S4 but for transcect 5 of the 2019 CALYPSO campaign.

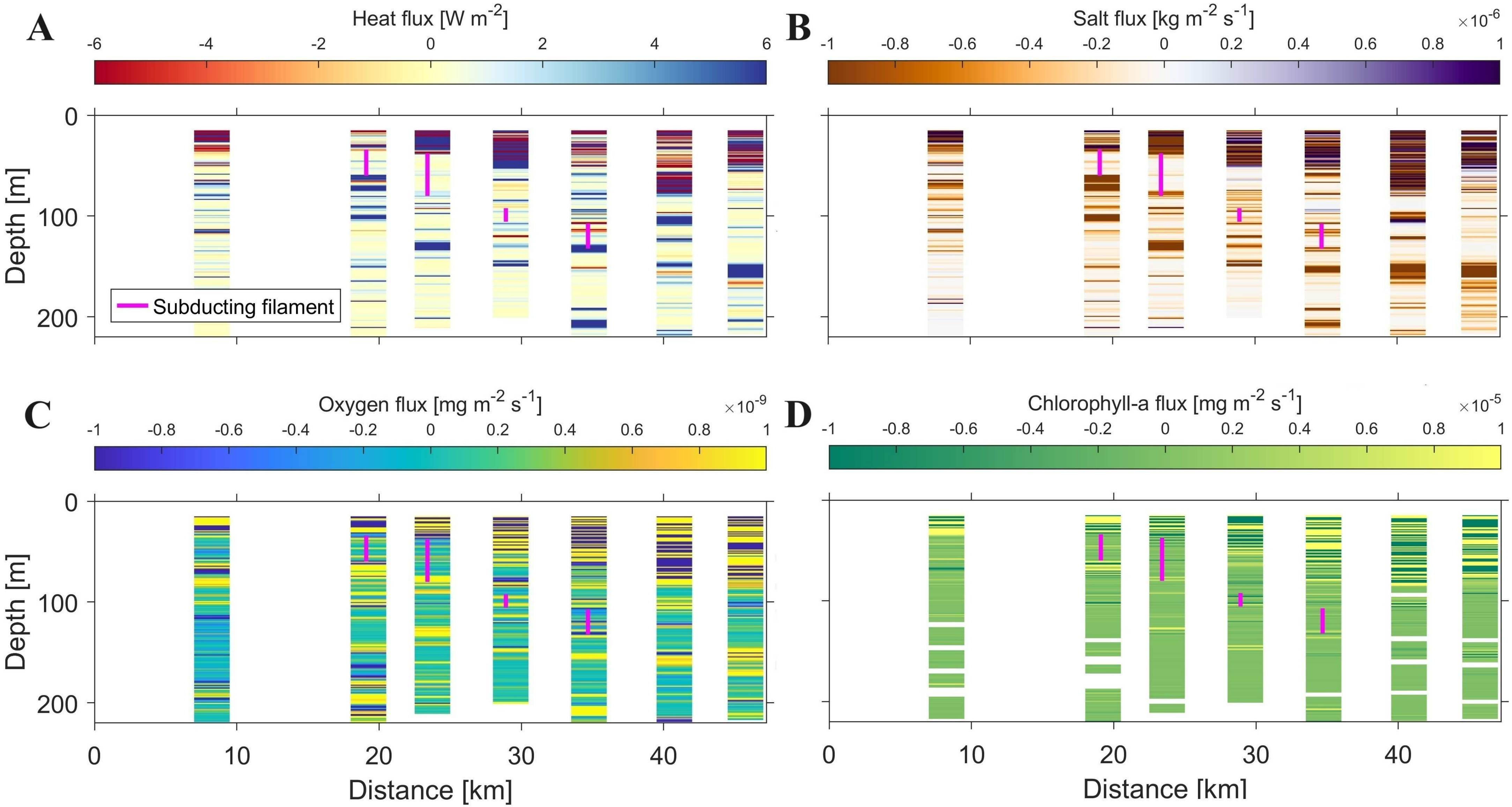

Figure S8. Heat **(A)**, salt **(B)**, dissolved oxygen **(C)** and chlorophyll-a **(D)** turbulent fluxes estimated along transect 2 of the 2019 CALYPSO campaign.

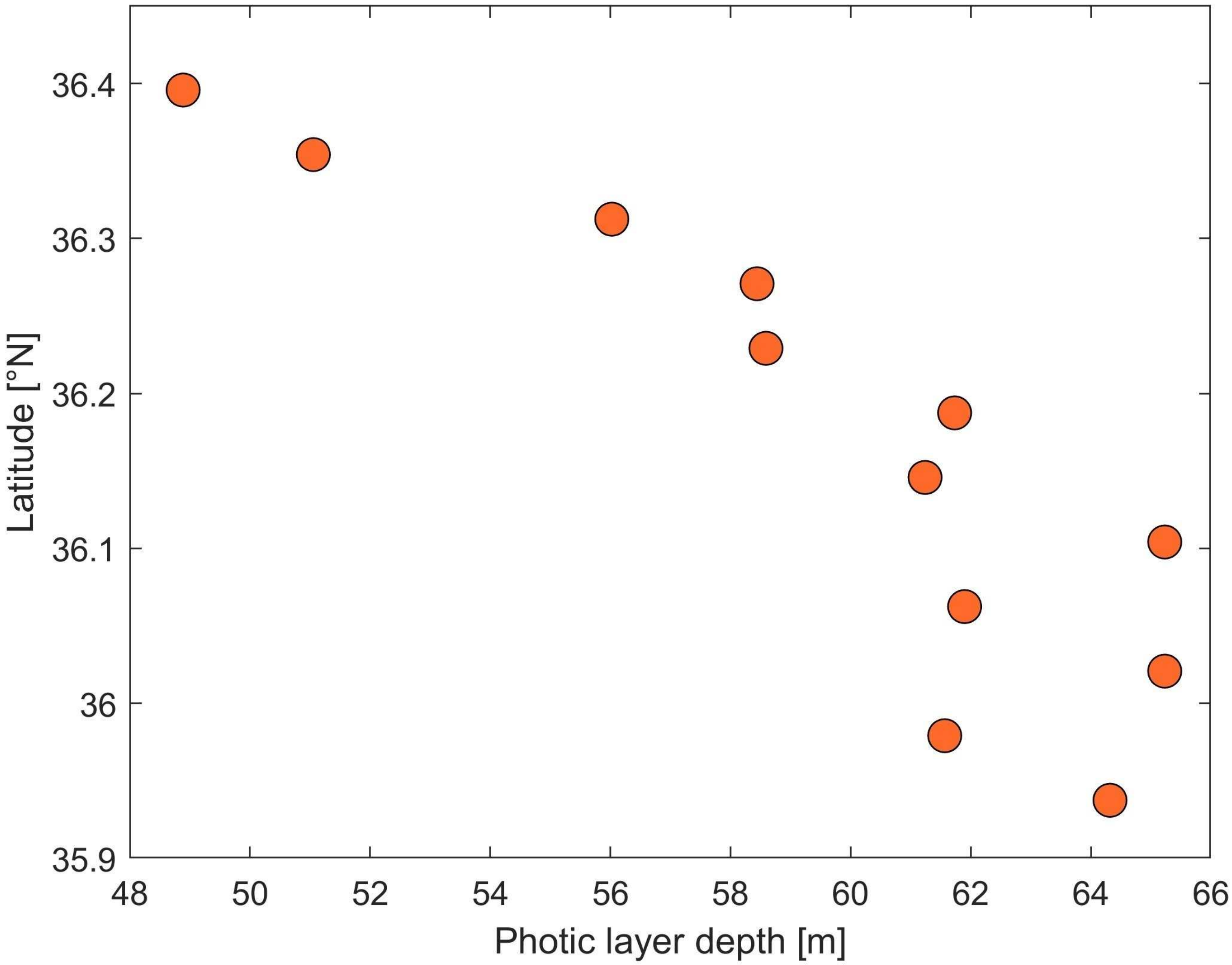

Figure S9. Satellite-derived photic layer depth variability along transect 2 of 2019 CALYPSO campaign. The meridional variability of the monthly composite (16th March-16th April 2019) at 4.1°W longitude is shown. Photic layer depth estimations (spatial resolution: 4 km) were computed from the diffuse attenuation coefficient data collected during the Aqua Moderate Resolution Imagining Spectroradiometer (MODIS) mission and following Behrenfeld *et al.* (2005; https://doi.org/10.1029/2004GB002299).

Table S1. Uncertainties assessment of turbulent fluxes of heat, salt, oxygen and chlorophyll-a along the upper and lower boundaries of the subducting intrusion identified within transect T2 of the 2019 CALYPSO campaign. The relative contributions of diffusivity (Kz) and the vertical variable gradient (∂X/∂z) to the total flux uncertainty are expressed as percentages.

Distance [km]	Boundary	Heat flux [W m^{-2}]	k_z [%]	∂T/∂z [%]	Salt flux [kg m^{-2} s^{-1}]	k_z [%]	∂S/∂z [%]	O_2 flux [mg m^{-2} s^{-1}]	k_z [%]	∂O_2/∂z [%]	Chl flux [mg m^{-2} s^{-1}]	k_z [%]	∂Chl/∂z [%]
0													
	Upper	22.8	98.9	1.1	$5.0 \cdot 10^{-7}$	98.7	1.3	$3.9 \cdot 10^{-9}$	81.3	18.7	$2.0 \cdot 10^{-5}$	94.4	5.6
	Lower	25.8	90.1	9.9	$2.6 \cdot 10^{-7}$	88. 4	11.6	$4.5 \cdot 10^{-9}$	55.9	44.1	$9.9 \cdot 10^{-6}$	74.7	25.3
4.3													
	Upper	4.7	76.3	23.7	$2.0 \cdot 10^{-7}$	95.8	4.2	$2.6 \cdot 10^{-9}$	74.1	25.9	$1.6 \cdot 10^{-5}$	84.0	16.0
	Lower	2.3	97.2	2.8	$1.8 \cdot 10^{-8}$	89. 5	10.5	$1.5 \cdot 10^{-9}$	88.0	12.0	$1.9 \cdot 10^{-6}$	80.6	19.4
9.8													
	Upper	0.9	78.7	21.3	$1.6 \cdot 10^{-8}$	93.2	6.8	$3.1 \cdot 10^{-10}$	14.3	85.7	$7.1 \cdot 10^{-7}$	27.6	72.4
	Lower	1.2	98.0	2.0	$7.7 \cdot 10^{-9}$	92.0	8.0	$2.2 \cdot 10^{-10}$	36.4	63.6	$7.0 \cdot 10^{-7}$	22.3	77.7
15.6													
	Upper	1.3	84.7	15.3	$1.3 \cdot 10^{-8}$	84.9	15. 1	$4.2 \cdot 10^{-10}$	1.7	98.3	$2.9 \cdot 10^{-7}$	1.5	98.5
	Lower	6.9	78.5	21.5	$1.7 \cdot 10^{-8}$	37.2	62.8	$2.0 \cdot 10^{-9}$	82.5	17.5	$8.3 \cdot 10^{-7}$	18.8	81.2

The uncertainty associated with turbulent was assessed by employing error propagation methods outlined in Taylor (1997). The standard deviation of each parameter involved in equations (6), (7) and (8) was utilized in this analysis. Furthermore, the propagation error calculation facilitates the assessment of the distinct contributions of various sources of uncertainty to the overall uncertainty. This information is crucial, as a heightened proportion of uncertainty attributed to diffusivity may signify an ambiguity in flux magnitude, while uncertainty primarily arising from variable vertical gradients may suggest uncertainty in flux sign determination.

Taylor, R.J., 1997. An Introduction to Error Analysis: The Study of Uncertainties in Physical Measurements. 2nd Ed., University Science Books